Journal of MATERIALS RESEARCH

Invited Feature Paper
DOI:10.1557/s43578-021-00433-w

Automated biofabrication of anisotropic dense fibrin gels accelerate osteoblastic differentiation of seeded mesenchymal stem cells

Gabriele Griffanti[1], Rayan Fairag[2], Derek H. Rosenzweig[2,3], Lisbet Haglund[2,3,4,5], Showan N. Nazhat[1,a)]

[1] Department of Mining and Materials Engineering, McGill University, 3610, University Street, Montreal, QC H3A 0C5, Canada
[2] Orthopaedic Research Laboratory, Division of Orthopaedic Surgery, McGill University, Montreal H3G 1A4, Canada
[3] Experimental Surgery, Department of Surgery, McGill University, Montreal H3G 1A4, Canada
[4] McGill Scoliosis and Spine Research Group, McGill University, Montreal H3G 1A4, Canada
[5] Shriners Hospital for Children, Montreal H4A 0A9, Canada
[a)] Address all correspondence to this author. e-mail: showan.nazhat@mcgill.ca

Received: 17 July 2021; accepted: 3 November 2021; published online: 23 November 2021

Current challenges in the biofabrication of stable, cell-seeded fibrin gels are faced with a lack of microstructural and mechanical properties, limiting their use as bone extracellular matrix-mimicking constructs. While current approaches focus on generating fibrin gels of various fibrinogen and thrombin concentrations, *i.e.* 5–50 mg mL^{-1} and 1–250 units mL^{-1}, respectively, processes that modulate gel fibrillar alignment and mechanical properties have yet to be explored. Herein, it was demonstrated that the automated gel aspiration-ejection (GAE) of precursor fibrin hydrogels of low concentration (*i.e.* 1 mg mL^{-1} fibrinogen and 0.5 units mL^{-1} thrombin) resulted in their immediate compaction while tailoring their fibrillar alignment and mechanical properties for potential target applications. Furthermore, this gel microenvironment accelerated the osteoblastic differentiation of seeded mesenchymal stem cells and their matrix mineralization, in vitro. Therefore, the ability to modulate the properties of dense fibrin constructs through automated GAE may be a novel biofabrication approach for cell delivery in bone regeneration.

Introduction

Bone is the second most transplanted tissue after blood [1]. Bone defects may be caused by ageing, tumour resection, congenital malformation, trauma, fractures, surgery or diseases such as osteoporosis or arthritis [2]. Autologous bone grafting, commonly from the patient's iliac crest, represents the gold standard for bone replacement. However, the supply of autogenous grafts is frequently scarce and a surgical approach is expensive, as well as being associated with a number of risks, including donor site morbidity, deformity and scarring [2].

Bioengineering approaches to overcome these problems include the development of novel biomaterials, protein and growth factor delivery, as well as gene or cell therapy [3]. Gene therapy and the delivery of proteins or growth factors are powerful only if there are cells in the defect sites able to respond to their signals [4]. When defects exceed a critical size, the local cell population is not sufficient to repair the injury and additional cells must be introduced. To this end, progenitor cells seeded into biocompatible and biodegradable scaffolds are grown ex-vivo and differentiated to mimic the native tissue. Moreover, recent advances in biofabrication have allowed for the production of reproducible and scalable tissue-like scaffolds used for in vitro tissue modelling, drug screening, as well as implantable constructs with tailored structural, biological and mechanical properties [5–7].

Fibrin is a naturally occurring biomaterial that acts as a scaffold for platelets, neutrophils, macrophages and endothelial cells during the formation or regeneration of tissues [8, 9]. Fibrin gels rapidly assemble, in vitro by a modified polycondensation reaction from fibrinogen, an abundant constituent of blood plasma. This occurs when the protease thrombin is activated in the clotting cascade, which removes the part of the fibrinogen

polypeptides that prevents its spontaneous polymerization [10]. As a biomaterial, fibrin has the main advantage of being produced directly from the patient's own blood and can be used as an autologous scaffold without the potential risk of rejection or infection [11]. Fibrin gels have been clinically applied as sealants [12] and as coatings on metallic [13] and synthetic polymeric [14, 15] implants to improve their biocompatibility. To date, fibrin gels have been produced through isolation of fibrinogen and thrombin, which are the mixed to generate gels, in vitro. The density (fibrin content) of the gels can be modulated by varying the fibrinogen and thrombin concentrations, with the former value often used to refer to this value. Fibrin gels have also been shown to promote the proliferation and osteoblastic differentiation of mesenchymal stem cells (MSCs), in vitro [16, 17]. In particular, fibrinogen and thrombin ranges from 5 to 50 mg mL^{-1} and 1 to 250 units mL^{-1}, respectively, have been used. It was shown that lower fibrinogen concentrations lead to higher MSC proliferation rates, whereas higher concentrations lead to their accelerated osteoblastic differentiation. Moreover, bioactive molecules [18, 19] and therapeutic cells [20–22] can be delivered through their incorporation into fibrin gels. However, the lack of control over the gel microstructure and mechanical properties poses limitations as scaffolds in cell delivery applications [11, 23–25].

While the mechanical properties can be improved by increasing the fibrin gel concentration, *e.g.* it has been reported that gel Young's modulus can range from 0.043 ± 0.016 to 0.974 ± 0.254 MPa by increasing the concentration from 5 to 50 mg mL^{-1} [26], the sterile filtration of the resulting gels would be extremely difficult [27]. On the other hand, a level of control over the fibrillar microstructure has been demonstrated by stretching the gel thus forcing the fibres to align along the direction of the applied force. However, this approach relies on the constant application of strain on the gel, thus requiring an *ad hoc* apparatus for the gel treatment and reproducing an environment which may not resemble the native condition [28]. Alternative approaches to improve the mechanical properties of fibrin gel consist of using crosslinkers, such as genipin. For example, it has been shown that the mechanical properties can be modulated by using different genipin concentrations without affecting seeded cell viability [29]. However, the use of crosslinkers did not enable control over the final construct fibrillar architecture. These drawbacks, along with the degradation of fibrin at high temperature, have severely limited its use in the biofabrication of bone-like structures [30]. For this reason, up to date, fibrin has only been used as coatings [31] or supporting materials [32, 33] for 3D printed composites used in bone-related applications.

Approaches to generating stable dense fibrin gels have included plastic compression (PC), which is a cell-friendly technique that has been extensively applied on highly hydrated collagen gels for the fabrication of compacted constructs with a microstructure characterized by randomly oriented fibrils and controllable mechanical properties [34–40]. Although the PC method has been successfully used on highly hydrated fibrin gels and shown to improve their mechanical properties through compaction while maintaining cell viability, this approach has yet to be explored for the production of bone mimicking structures and is not automatable [27]. Gel aspiration-ejection (GAE) is an alternative technique that has been used to increase the fibrillar density and alignment of collagen gels [41, 42]. Moreover, this approach has recently been automated through the use of a customized instrument in order to rapidly and reproducibly fabricate compacted and anisotropic collagen mini-tissue building blocks with tailorable properties such as shape, volume, density, fibrillar alignment and mechanical properties [43]. Through this approach, precursor highly hydrated collagen gels are aspirated into blunt-tip needles of a predefined lumen size by application of negative pressure, and ultimately ejected by reversing the pressure, thus producing dense collagen gels that can be used as mini-tissue building blocks and assembled to build more complex structures. Interestingly, gel properties can be predicted by using a simple mathematical relationship based on a compaction factor occurring during automated GAE biofabrication [43].

In order to overcome the limitations described above in generating stable fibrin gels as scaffolds for bone tissue engineering, this study applied automated GAE to design dense fibrin gels with tailored microstructural and mechanical properties. Automated GAE was applied on precursor highly hydrated fibrin gels characterized by low fibrinogen and thrombin concentrations, thereby negating the need of gels with high fibrinogen concentrations and allowing for an easy sterile filtration process for cell-based applications. By using needles of different lumen sizes, gels of distinct densities and microstructures were simultaneously generated. In addition, the viability, proliferation, remodelling activity, osteoblastic differentiation and matrix mineralization capacity of MSCs seeded in automated GAE-enabled gels were compared to those seeded in PC-generated constructs. PC-generated constructs were also considered not only as a control with a different fibrillar architecture, but also in order to assess their potential in bone tissue engineering applications.

Results

Characterization of dense fibrin gels

The application of both automated GAE and PC led to the production of compacted, dense fibrin gels as a consequence of the expulsion of casting fluid from precursor gels. Automated

GAE-generated gels, GAE-DF-88% and GAE-DF-95%, were of fibrillar densities of 5.53 ± 0.75 and 10.14 ± 1.47 wt%, respectively, while PC-DF gels were characterized by a fibrillar density of 10.00 ± 1.12 wt%.

In terms of morphology, automated GAE and PC generated dense fibrin gels of distinct architectures. At the macroscale, PC-DF gels appeared as thin sheets (Fig. 1a) compared to the cylinder-shaped GAE-DF gels (Figs. 1b, c) produced by automated GAE, where the size was dependent on the needle gauge number. At the microscale, SEM images displayed a more random orientation of fibres in PC-DF, organized in a mesh-like structure (Fig. 1a), whereas images of GAE-DF gels displayed different extents of fibrillar anisotropy, which in turn depended on the compaction factor, or surface area reduction; SAR% (Figs. 1b, c). While the fibres in GAE-DF-88% were less compact and randomly oriented (Fig. 1b), those in GAE-DF-95% were organized in bundles with a neat preferential orientation (Fig. 1c). Fibre orientation, as defined by directionality, was quantified from the SEM images (Fig. 1d). The Gaussian distributions in PC-DF and GAE-DF-88% were broad, indicating low fibre directionality, whereas there was a narrower distribution in GAE-DF-95%, indicating a greater extent of fibrillar alignment and anisotropy. This extent of fibrillar alignment was reflected in the tensile stress–strain curves, which displayed distinct mechanical properties for PC-DF, GAE-DF-88% and GAE-DF-95%, with the latter presenting significantly higher ($p < 0.05$) ultimate tensile strength (UTS) and apparent modulus values (Fig. 1e). In particular, PC-DF, GAE-DF-88% and GAE-DF-95% were characterized by a UTS mean value of 0.133 ± 0.005, 0.056 ± 0.007 and 0.215 ± 0.048 MPa; and an apparent modulus mean value of 0.492 ± 0.114, 0.135 ± 0.028 and 0.874 ± 0.145 MPa.

Seeded MSC proliferation and osteoblastic differentiation in gels

In order to assess the potential of dense fibrin gel gels as scaffolds for bone tissue engineering, the function of seeded MSCs in both GAE-DF-88% and GAE-DF-95.33% were compared to those seeded in PC-DF. The effect of scaffold architectural properties on cell viability, proliferation, remodelling activity (as measured through cell-induced gel contraction) and osteoblastic differentiation was evaluated up to 28 days in culture. CLSM images of calcein AM-stained cells showed extensive viability where cells were temporally and spatially growing in all gels, independent of culturing media (Fig. 2). Cells seeded in GAE-DF-95% in basal medium appeared to be polarized preferentially along the longitudinal axis of the gel up to day 7. In contrast, cells seeded in PC-DF and GAE-DF-88% were not preferentially oriented within the same time frame.

Seeded MSC-mediated gel remodelling activity was evaluated up to 21 days in basal and osteogenic media. Gel images taken immediately after fabrication (day 0) and at day 21 in culture (Fig. 3a; top and bottom, respectively) revealed different levels of contraction, which were dependent on culturing media and SAR%. Changes in cell-mediated gel contraction (Fig. 3b; left and right panels, respectively) followed a sigmoidal trend,

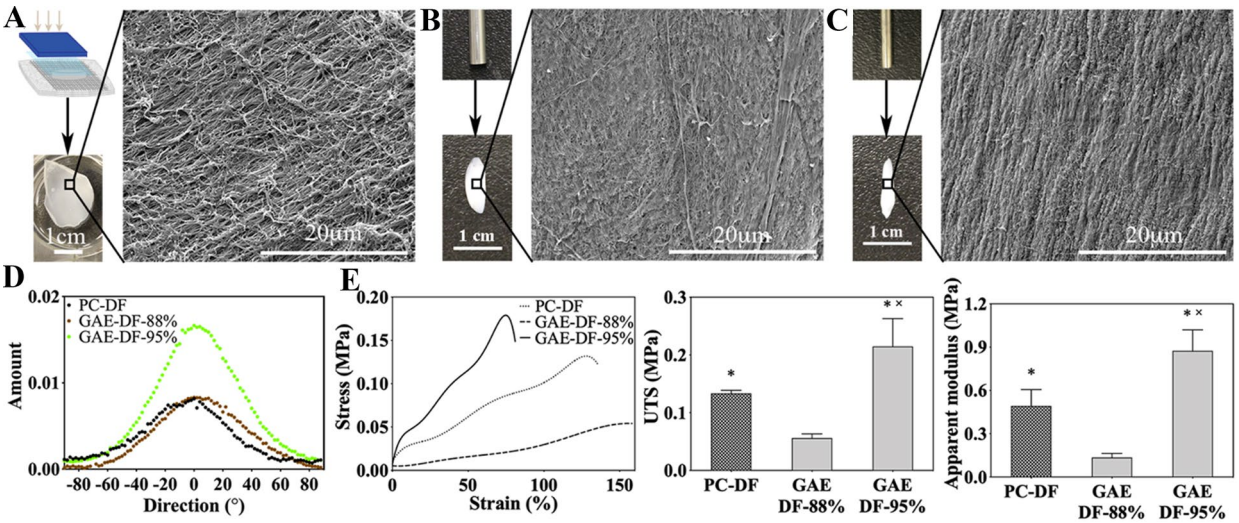

Figure 1: Macro-to-micro-architectural and mechanical properties of dense fibrin gels. Macro-to-microscale images of (a) PC-DF, (b) GAE-DF-88% and (c) GAE-DF-95%. While PC-DF and GAE-DF-88% fibres were characterized by more random orientation, GAE-DF-95% fibres appeared to be organized in bundles with a preferred orientation. (d) Gaussian distribution of fibre directionality generated from SEM micrographs. Gaussian distribution appeared narrower with the increase in SAR%. PC-DF was used as control. (e, left) Representative tensile stress–strain curves of PC-DF and GAE-DF gels, (middle) UTS and (right) apparent modulus calculated from the stress–strain curves, indicating significantly greater values in GAE-DF-95% compared to GAE-DC-88% (*$p < 0.05$) and PC-DF (×, $p < 0.05$), respectively.

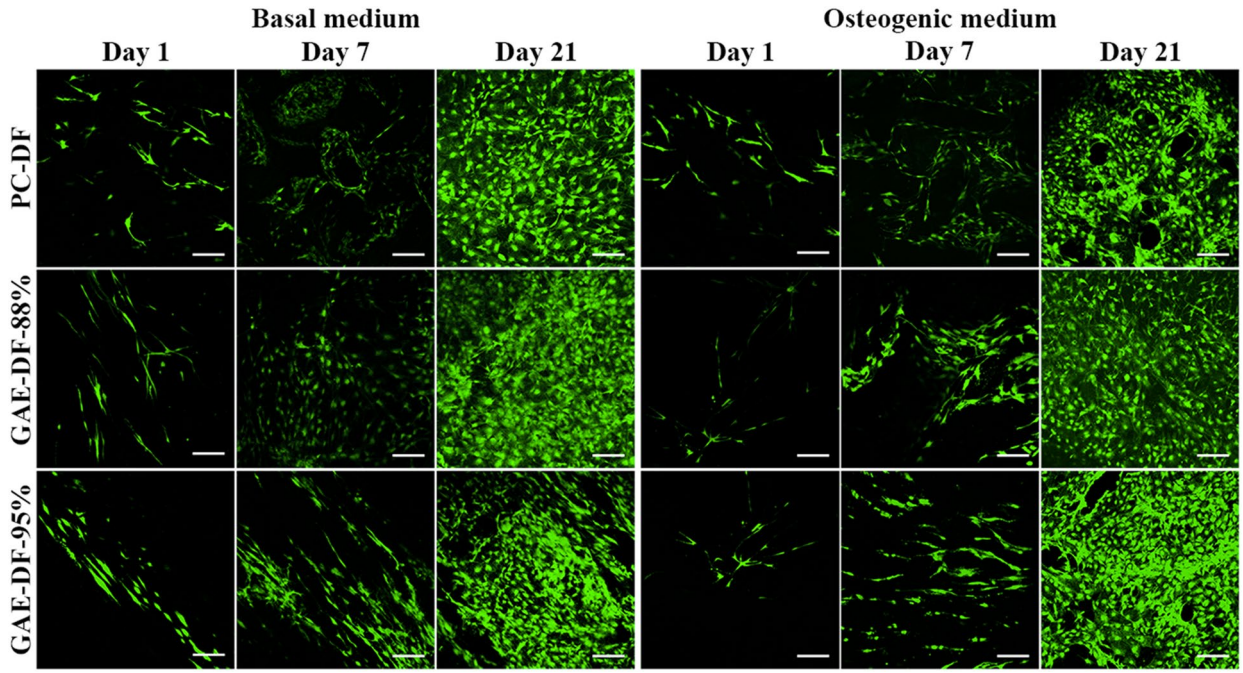

Figure 2: CLSM images of calcein AM-stained MSCs cultured in PC-DF, GAE-DF-88% and 95% at days 1, 7 and 21 under basal and osteogenic media. MSCs were observed to be temporarily and spatially growing in all gels. Scale bar = 150 μm.

where there was a decrease in gel surface area until day 11 in both conditions reaching a stable level of contraction. In basal medium, while GAE-DF-88% underwent a prominent level of contraction, PC-DF and GAE-DF-95% contracted to a lesser extent. In addition, the onset of contraction in GAE-DF-95% was delayed to day 7 in culture in basal medium (Fig. 3b; left). Under osteogenic medium, contraction in GAE-DF-88%, PC-DF and GAE-DF-95% was delayed until days 5, 7 and 9, respectively (Fig. 3b; right) and was significantly ($p < 0.05$) lower when compared to that observed in gels cultured in basal medium. In contrast, there was no detectable contraction in acellular gels over the same period under both media (Fig. S1).

Cell metabolic activity increased in all gels in both basal and osteogenic media up to day 14, suggesting an increase in MSC proliferation rate. However, at day 21, MSCs cultured in basal medium presented significantly ($p < 0.05$) higher metabolic activity compared to those cultured in osteogenic medium. In basal medium, the metabolic activity of MSCs at day 21 in all gels reached a similar level while the intermediate points showed differences indicating different proliferation rates both at days 7 and 14. In osteogenic medium, MSCs seeded in PC-DF exhibited an increasing trend between days 1 and 21, whereas those in GAE-DF-88% and GAE-DF-95% stabilized and decreased between days 14 and 21, respectively. In addition, the metabolic activity of cells seeded in PC-DF was significantly lower than in GAE-DF-88% and GAE-DF-95% at day 14 (Fig. 4a).

q-PCR analysis was performed at days 7, 14 and 21 and the levels of expression of *Alp*, *Runx2, Ocn* and *Col1a1* were evaluated as an indicator of osteoblastic differentiation. When cultured in osteogenic medium, the levels of expression of all four genes were significantly higher than in basal medium, suggesting MSC osteoblastic differentiation in all gels. MSCs seeded in PC-DF gels and GAE-DF-88% and cultured in osteogenic medium did not display statistically significant ($p > 0.05$) differences in the levels of expression of *Alp*, *Runx2* and *Ocn* and *Col1a1* at all time points. However, MSCs seeded in GAE-DF-95% showed a significantly ($p < 0.05$) higher expression in *Alp* at day 14, and in *Runx2* and *Ocn* at days 14 and 21 compared to MSCs seeded in PC-DF and GAE-DF-88% (Fig. 4b).

Protein analysis at day 28 confirmed the osteoblastic differentiation of seeded cells (Fig. 5) along with cell-mediated mineralization of the constructs as evaluated through SEM, ATR-FTIR spectroscopy and XRD (Fig. 6). Densitometry analysis through western blotting revealed the production of OPN in all cell-seeded gels, in particular under osteogenic medium (Figs. 5a, b). There was a greater fold increase in GAE-DF-95% followed by GAE-DF-88% and PC-DF (Fig. 5c). SEM micrographs showed particle deposition in MSC-seeded PC-DF and GAE-DF-95% while no deposition was observed in GAE-DF-88% (Fig. 6a). Qualitatively, particle size appeared greater in MSC-seeded GAE-DF-95% compared to PC-DF. ATR-FTIR spectroscopy revealed absorption bands at 1626, 1511 and 1220 cm^{-1}, which represented the characteristic peaks of fibrin, *i.e.* Amide I, II and III, respectively. An increase in the absorption bands related to phosphorous groups, which can be correlated with mineral deposition, were found in the 1100–1000 cm^{-1} interval in

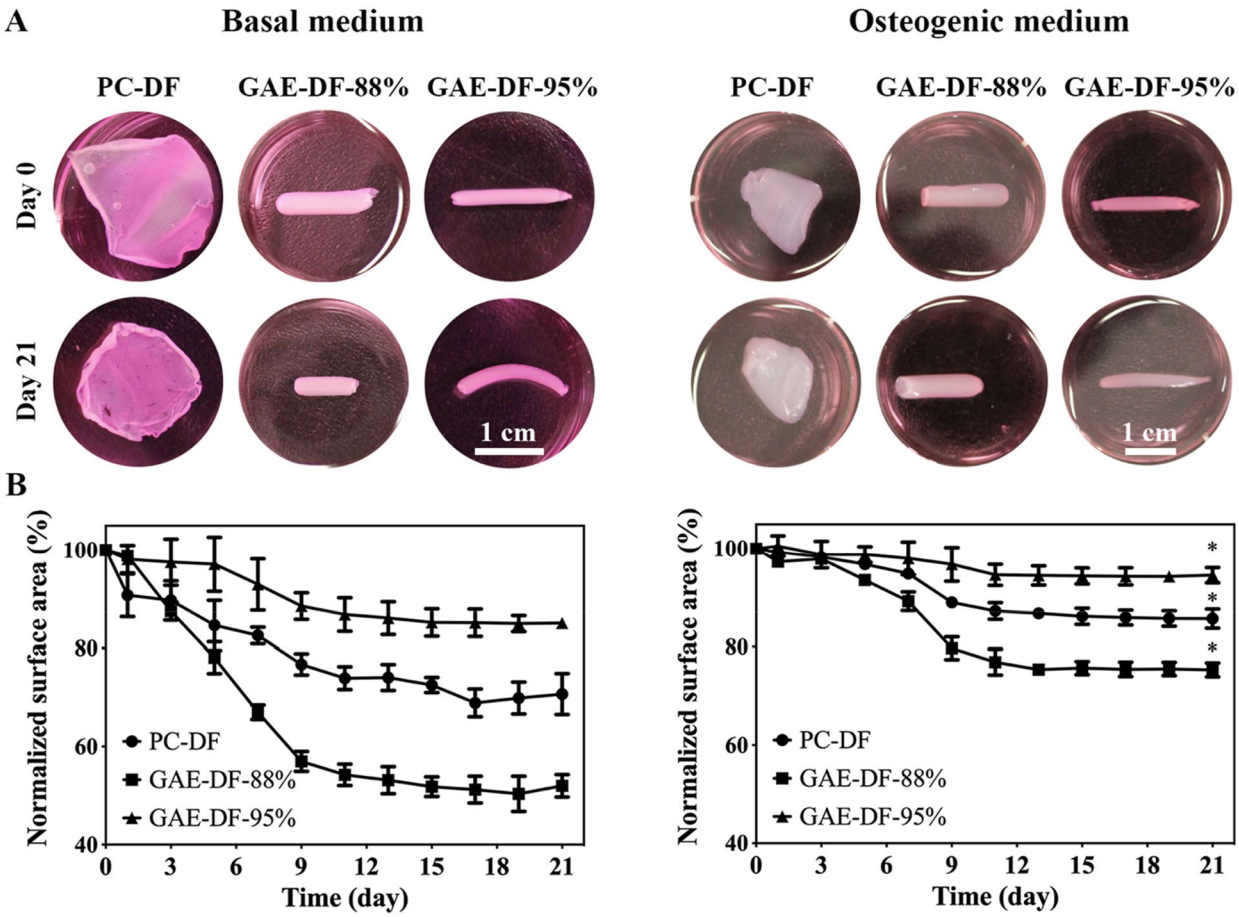

Figure 3: MSC-induced gel contraction of PC-DF, and GAE-DF-88% and GAE-DF-95% up to day 21 in basal and osteogenic media. (a) Macroscopic images of gels at days 0 and 21 in culture in basal (left) and osteogenic (right) media. (b) Quantification of gel compaction up to day 21 in culture in basal (left) and in osteogenic (right) media. Contraction of GAE-DC-88% was more pronounced than PC-DF and GAE-DC-95%. Extent of contraction was lower in osteogenic medium, which stabilized after day 11. Contraction was not observed in acellular gels for either medium condition (Fig. S1). *Significantly ($p < 0.05$) lower contraction when compared to the corresponding sample in basal condition.

MSC-seeded PC-DF and GAE-DF-95%. XRD diffractograms indicated the formation, or an initial transition towards an apatite phase in MSC-seeded GAE-DF-95% only, attributable to the presence of a peak around 32° 2θ degree. In contrast, analysis of MSC-seeded gels at day 28 in basal medium did not indicate mineral deposition (Fig. S2).

Discussion

This study has demonstrated that automated GAE can be applied to produce dense fibrin gels of tailorable microarchitectures and mechanical properties. By simply introducing an aspiration step on prefabricated precursor gels, automated GAE imparts both compaction and anisotropy prior to the ejection of dense fibrin gels. Furthermore, the automated GAE-designed gels supported the osteoblastic differentiation of seeded MSCs and may represent a promising strategy to deliver therapeutic cells for bone tissue engineering.

Strategies to improve the mechanical properties of fibrin gels have been explored by altering the fibrinogen and thrombin concentrations [44, 45]. However, the challenge in the sterile filtration of high fibrinogen concentrations limits their cellular applications. Additionally, this approach does not allow for the controlled biofabrication of fibrous architectures. Fibrin gels characterized by low gel concentrations have been used to produce structures resembling those of neural tissues [46–48], tympanic membranes [49], as well as models to study possible therapies for glioblastoma tumours [50]. However, to date, fibrin gels have not been used to produce bone-like structures, which may be due to the difficulties in directly handling highly concentrated fibrin gels in a controllable manner and with architectural properties similar to those of the native tissue; a hierarchically organized mineralized fibrillar collagen network [51, 52]. While fibrin gels are characterized by a mesh-like fibrous structure [28], their highly hydrated nature corresponds to relatively weak mechanical

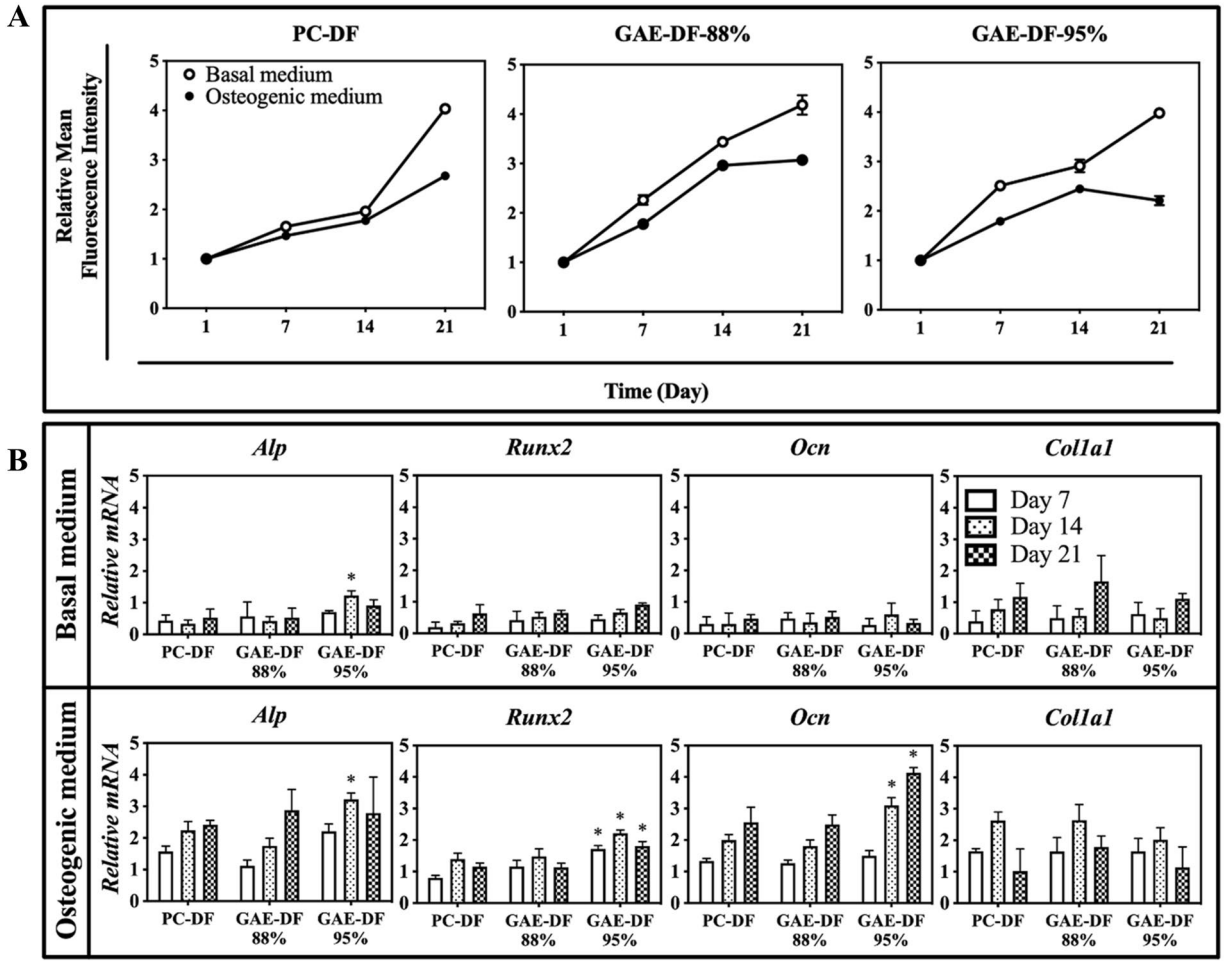

Figure 4: Seeded MSC metabolic activity and osteogenic differentiation. (a) MSC metabolic activity seeded in PC-DF, GAE-DF-88% and GAE-DF-95% and cultured up to day 21 in basal and osteogenic media. MSC metabolic activity under basal medium increased up to day 21 in all gels. MSC metabolic activity under osteogenic medium reached a plateau and decreased at day 21 in GAE-DF-88% and GAE-DF-95%, respectively. (b) Expression of *Alp*, *Runx2*, *Ocn* and *Col1a1* genes in MSCs cultured in PC-DF, GAE-DF-88% and GAE-DF-95% at days 7, 14 and 21 in basal and osteogenic media. Under basal medium, the expression of *Alp* in MSCs was higher ($p < 0.05$) in GAE-DF-95% at day 14 when compared to the other gels. Under osteogenic medium, *Alp* (at day 14), *Runx2* (at days 7, 14 and 21) and *Ocn* (at days 14 and 21) expression was higher ($p < 0.05$) in MSCs seeded in GAE-DF-95% compared to the other gels.

properties, which impacts their physiological relevance as bone extracellular matrix (ECM)-mimicking constructs [52]. Therefore, the use of fibrin in bone tissue engineering has been limited to coatings [31] or supporting [32, 33] materials.

In this study, the structural and mechanical properties of automated GAE-generated dense fibrin gels were compared to PC-generated gels. These two approaches rely on the controlled expulsion of the casting fluid from precursor gels produced with a low fibrinogen concentration, while generating different fibrillar architectures. PC, which has been widely used with collagen gels [34], and successfully applied on fibrin gels [27], results in gels characterized by a randomly oriented fibrillar structure. In contrast, automated GAE-generated gels can be characterized by both, higher densities and different extents of anisotropy, as dictated by the SAR%. These observations are in line with those generated in dense collagen gels [42, 43] thus confirming that automated GAE and SAR% can be successfully applied to other fibrous hydrogels. SAR represents a simple yet powerful tool to predict and tailor the architectural (fibrillar density and orientation) and mechanical properties of gels in order to meet those of the target tissue. Therefore, automated GAE represents an appealing alternative to modulating either the fibrinogen concentration [16, 53–55] or extent of fibre alignment through the application of uniaxial stress [28]. This densification of the fibrillar network results in an increase in contact points between the fibres, thereby requiring higher tensile stresses to induce deformation [42]. Interestingly, tensile stress–strain curves highlighted the effects of the distinct fibrous architectures of PC-DF and GAE-DF-95%. While both gels were of similar density, the

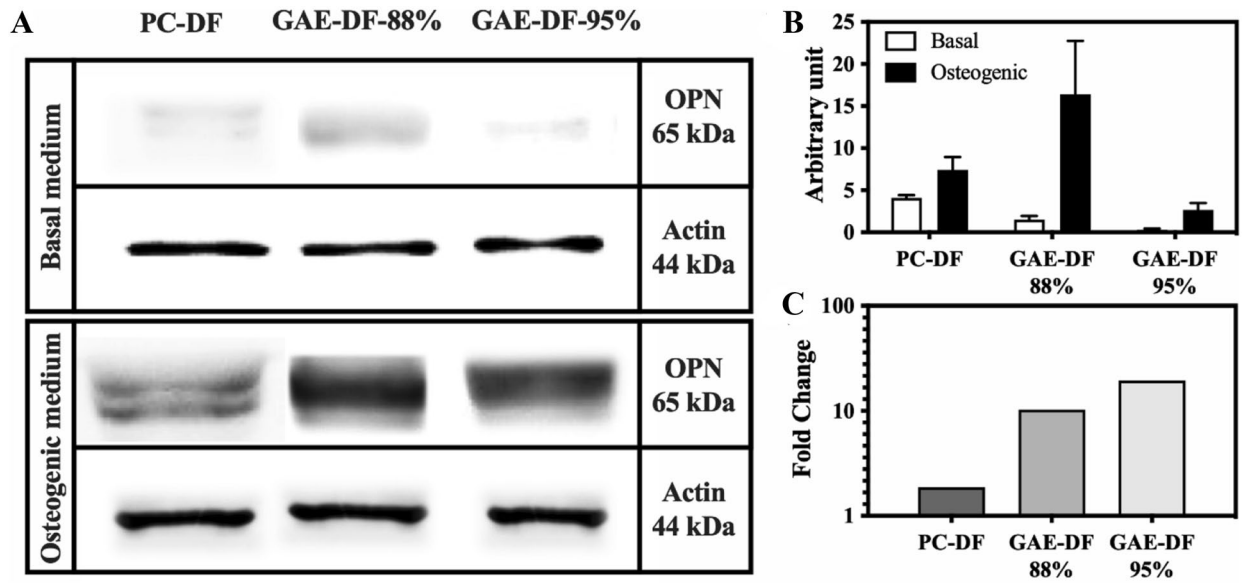

Figure 5: OPN production in seeded MSCs. (a) Representative Western blot of OPN accumulation, (b) densitometry quantification and (c) fold change from basal to osteogenic media cultures of seeded gels.

increased extent of fibre alignment in GAE-DF-95% generated higher apparent modulus and strength values, which can be attributed to a greater number of fibres recruited along the tensile force [56]. Furthermore, considering that the initial concentration of fibrinogen in the highly hydrated precursor was 1 mg mL^{-1}, the higher modulus value demonstrated by GAE-DF-95% post automated GAE (0.874 ± 0.145 MPa), is similar to what was previously reported for fibrin gels produced using an initial fibrinogen concentration of 50 mg mL^{-1} (0.974 ± 0.254 MPa) [26]. However, the latter is limited in terms of cellular-based applications as its concentration hinders the sterile filtration process, thus emphasizing the novelty of GAE as a cell-friendly process for the production of fibrin gels with improved mechanical properties.

The fabrication of an endogenous fibrin gel with a native bone ECM-like structure that promotes the rapid expansion of seeded cells is critical for potential clinical applications [26]. It has been demonstrated that the use of molecules found in provisional wound healing types of matrices may better mimic the natural process of bone repair [57]. Fibrin, in particular, plays a pivotal role in wound healing, acting as a scaffold for cell migration, adhesion and differentiation [58]. Bulk and local scaffold properties can also direct cell behaviour, where cellular activities (*e.g.* attachment, migration and differentiation) can be directed by matrix stiffness [59–62]. Previous studies have shown that the proliferation and differentiation of seeded MSCs are affected by the fibrinogen concentration, which controls the density of the fibrin gel [16, 53]. When the fibrinogen concentration is low, the resulting fibrin gel is loose and MSC proliferation is high [53], whereas when the fibrinogen concentration is high, the gel is denser, which in turn decreases MSC proliferation and increases osteogenic differentiation [16, 53].

This study evaluated the osteogenic differentiation of seeded MSCs in automated GAE-generated gels and compared these to MSCs seeded in PC-DF gels. Previous work on collagen, demonstrated that SAR values corresponding to 88 and 95% improved the osteoblastic outcomes of seeded MSCs [42]. Furthermore, a SAR value higher than 95% may be detrimental to cell viability when seeded in collagen [43]. For this reason, the same SAR values were used in this work with fibrin. Moreover, PC-DF and GAE-DF-95% provided a platform to investigate the osteogenic differentiation pathway in gels characterized by similar density, but different fibrillar architectures (*i.e.* random oriented versus anisotropic). While MSCs were found to adhere and proliferate in all gels, cells seeded in GAE-DF-95% were oriented axially along the fibrin bundles as dictated by the aspiration direction. This type of cell polarization was not observed in neither PC-DF nor GAE-DC-88%, where cells appeared randomly oriented. Therefore, cell polarization appeared to be dictated by SAR as has also been demonstrated in dense collagen gels [43]. However, by day 21, cell polarization was no longer observed due to widespread cell proliferation.

No qualitative gel degradation was observed after 21 days in culture, attributable to the addition of aprotinin, a proteinase inhibitor that prevents fibrinolysis, and commonly used to delay fibrin-based scaffold degradation [63, 64]. However, fibrinolysis is likely to also have been delayed due to the deposition of nascent ECM components from seeded cells, which has been demonstrated to hinder fibrinolytic enzyme action, thus stabilizing the fibrin network [65, 66]. Seeded MSC remodelling activity

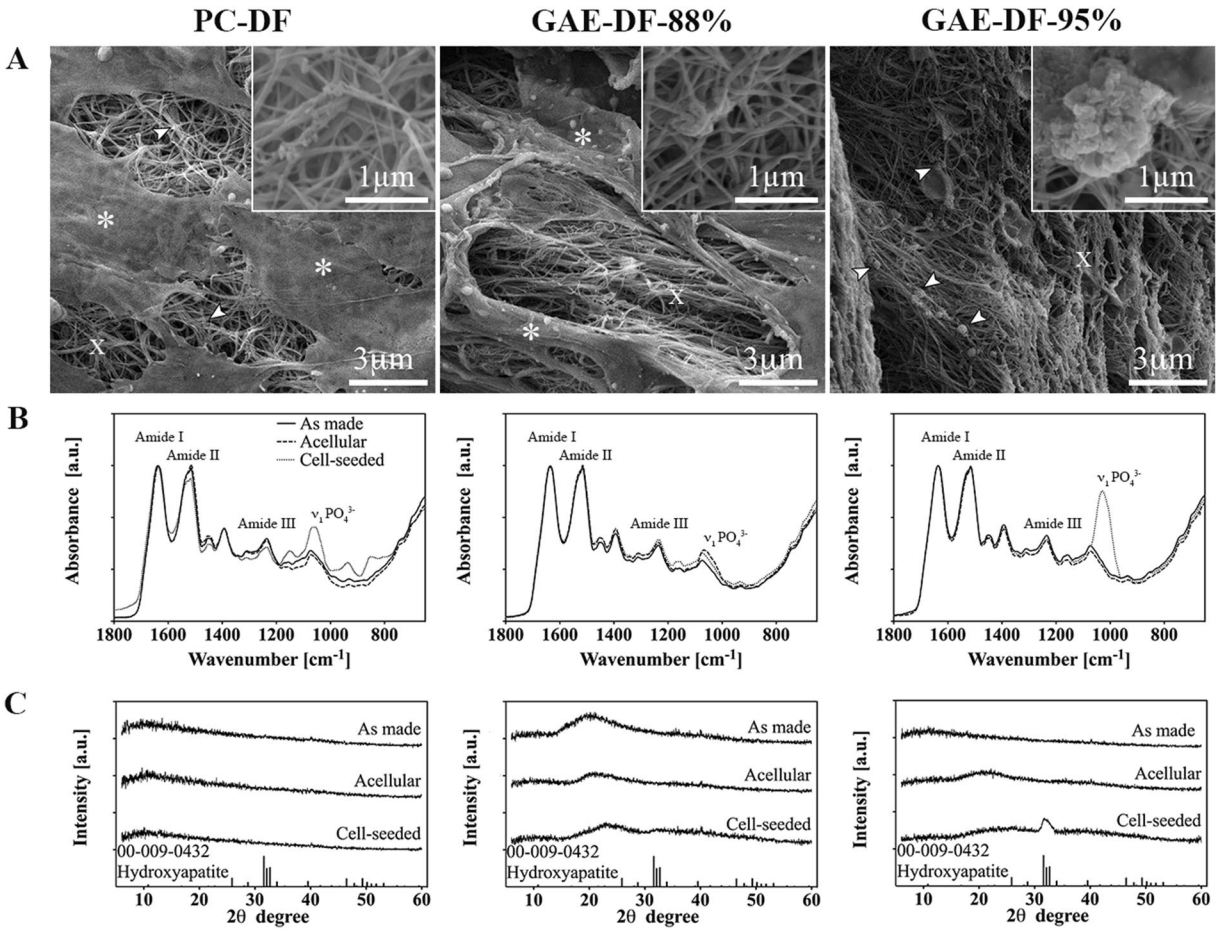

Figure 6: Cell-mediated mineralization. Characterization of mineral deposition at day 28 in osteogenic medium. (a) SEM micrographs showing particle deposition in PC-DF and GAE-DF-95% (highlighted by white arrows and in insert), cells (highlighted by white *) and fibrous matrix (highlighted by white X). (b) ATR-FTIR spectra of the as-made, acellular and cell-seeded gels revealed increased intensities of absorption bands corresponding to phosphate groups in cell-seeded PC-DF and GAE-DF-95%. (c) XRD diffractograms of the as-made, acellular and cell-seeded gels showed amorphous patterns for all PC-DF and GAE-DF-88% while the presence of a peak at 32 2θ degree, which can be associated with an early stage of transition towards a crystalline apatite phase, was observed in GAE-DF-95% only. The diffraction pattern of hydroxyapatite is used as reference. SEM micrographs, ATR-FTIR spectra and XRD diffractograms of samples cultured in basal medium are provided in Fig. S2.

not only induces gel contraction but also results in the secretion of ECM components to support cell survival, proliferation and differentiation [67]. Cell-induced gel contraction has been reported in fibrin [54], where cells exert mechanical forces on the surrounding fibrillar network to reach physiological protein concentrations [68]. In this study, the onset and extent of cell-induced gel contraction was dependent on fibrin fibrillar density, which appeared to be delayed in gels with higher density, similar to previous findings on plastically compressed [69–71] and automated GAE-generated [43] dense collagen gels.

It is known that scaffold remodelling does not occur when the matrix stiffness exceeds cellular contractile forces, and the fibrin gel density has been shown to affect the extent of cellular contractility [28, 54, 55]. In this study, the increased stiffness in denser constructs counteracted the cellular contractile forces and decreased the extent of contraction. Lower cell-induced contraction was also observed in gels cultured in osteogenic medium. This may be due to the reduced proliferation and migration of seeded MSCs [69]. Indeed, MSC metabolic activity was higher when cultured in basal medium, reflecting a higher proliferation rate of undifferentiated cells [72–74]. Furthermore, MSC metabolic activity at day 14 in both basal and osteogenic media was higher when seeded in GAE-DF-88% compared to the other gels, echoing previous findings where the proliferation of cells, such as fibroblasts and MSCs, seeded in fibrin gels decreased with increased fibrinogen concentration and therefore fibrin density [26, 27, 53]. In contrast, the lower proliferation rate of MSCs seeded in PC-DF and GAE-DF-95% may be due to their accelerated differentiation as a consequence of increased construct densities [16, 53]. Indeed, the expression profiles of *Alp*, *Runx2*, *Ocn* and *Col1a1* genes were investigated to assess the effects of fibrin gel density and anisotropy on MSC osteoblastic

differentiation. *Alp* is an early marker in the osteogenic pathway, and is implicated in bone formation and mineralization [75]. *Runx2* is a marker associated with the osteoblast lineage, which activates and regulates the expressions of *Col1a1* [76] and osteoblast-specific gene *Ocn*. *Ocn*, in turn, is a tissue-specific gene expressed only by mature osteoblasts [77], while *Col1a1* gene expression is expressed when cells secrete their own ECM that is dominated by type I collagen, which templates mineral formation and regulates mineralized tissue homeostasis, thus promoting the differentiation and growth properties of osteoblast-like cells [78].

Osteoblastic differentiation in vitro is characterized by a temporal pattern of gene expression, where in the early stages, cells grow and synthetize type I collagen to support proliferation and matrix formation. On the other hand, an upregulation of *Alp* indicates the cessation of cellular growth and the maturation of the deposited ECM. At longer times in culture, proteins with a high affinity to the mineral phase in bone such as osteocalcin are expressed at the onset of mineralization [77]. Interestingly, at day 14 in basal medium the expression of *Alp* in MSC-seeded GAE-DF-95% was higher than those seeded in PC-DF and GAE-DF-88%, suggesting that this gel architecture affected gene expression. Furthermore, while all four genes were expressed by MSCs in osteogenic medium, and although the densities in PC-DF and GAE-DF-95% were similar, an accelerated osteoblastic differentiation was observed in MSCs when seeded in GAE-DF-95%, which may be attributed to their distinct fibrillar alignment. While it has been shown that fibrin gel density modulates MSC osteoblastic differentiation [16, 53] and MSCs seeded in aligned fibrin gels expressed enhanced osteoblastic outcomes compared to those seeded in randomly oriented gels [28], the results in this study suggest a synergic effect of both fibrillar density and alignment.

Previous works have demonstrated that the expression of *Ocn* stabilizes upon the onset of matrix mineralization [73, 79–81]. However, at day 21 in osteogenic medium, cells seeded in all gels exhibited a higher level of *Ocn* expression compared to day 14, thus suggesting that mineral deposition was not occurring at this time point. For this reason, expression of OPN was investigated at day 28 as a late marker of mineralization and osteoblast-mediated mineral deposition [82]. Interestingly, OPN was also detected in basal medium, suggesting that the dense fibrin gels may recapitulate the properties of the native microenvironment [41]. Moreover, under osteogenic medium, the fold change in OPN was higher in MSCs seeded in GAE-DC-95%, thus supporting the hypothesis that the higher density and extent of anisotropy better supported their osteogenic differentiation and mineralization. Indeed, while phosphate-based mineral deposition was detected in both PC-DF and GAE-DF-95%, a clear peak at 32 2θ degree was observed only in the latter. This peak is one of the dominant peaks within the diffractogram of apatite, and its presence suggests the possible initial transitioning of the mineralized matrix towards a more mature crystalline structure in GAE-DF-95%, thus supporting their accelerated osteoblastic differentiation.

Conclusions

Biofabricated dense fibrin gels with well-defined microstructure and mechanical properties were enabled through automated GAE, a technique that simultaneously controls construct fibrillar content and alignment. It was shown that the aspiration of precursor gels characterized by a low concentration (*i.e.* 1 mg mL^{-1} fibrinogen and 0.5 units mL^{-1} thrombin) through a capillary offered advantages, in terms of both compaction and modulation of the fibrillar structure, thereby enabling the design of different levels of anisotropy. In particular, GAE-DF-95% displayed mechanical properties similar to those of previously reported fibrin gels characterized by high concentrations (*i.e.* 50 mg mL^{-1} fibrinogen and 250 units mL^{-1} thrombin). Furthermore, the ability of the GAE-DF gels to support seeded MSC adhesion, proliferation and modulate their osteoblastic differentiation depending on their properties, in vitro, has potential in bone tissue engineering applications. For example, the densities and fibrillar alignment levels of native tissues can be mimicked and replicated through this approach. Gels with native-like structures can then be used not only to model physiological processes such as bone formation and/or remodelling, but also to replicate pathological conditions. Moreover, while more detailed pre-clinical studies with resolution techniques and animal models are needed to confirm these in vitro observations, it can be postulated that automated GAE offers promise as a novel biofabrication approach in the development of endogenous gels for cell delivery in bone regeneration.

Materials and methods

Preparation of precursor highly hydrated fibrin hydrogels

Fibrinogen powder (Type I-S, 65–85% protein, Sigma-Aldrich, Canada) was dissolved in phosphate buffered saline (PBS) solution to a final concentration of 1 mg mL^{-1} and mixed with 0.5 U mL^{-1} thrombin solution (40–300 NIH units/mg protein, Sigma-Aldrich, Canada). Aliquots of 1.5 mL were then subdivided into a 48-well plate mould (Corning Costar, USA) and incubated at 37 °C for 20 min to induce the polycondensation reaction of fibrinogen and gelation and produce the precursor highly hydrated fibrin hydrogels, which were then subjected to either automated GAE or PC, as described below.

Automated GAE-generated dense fibrin gels

Automated GAE was applied on as cast, cylindrical precursor highly hydrated fibrin hydrogels to generate dense fibrin (GAE-DF) gels (Fig. 7, Video S1). A syringe pump (GeSim mbH, Germany) filled with an incompressible fluid (*e.g.* water, PBS, culture media) necessary for gel ejection was used to apply pressure differentials. Needle gauge numbers of 8G and 12G (of diameters 3.43 and 2.16 mm, respectively) were attached to the syringe pump through a Luer lock connector. The flow direction and rates were controlled through the instrument software. The automated GAE process was initiated by gently positioning the attached needle at the concentric surface centre of the precursor gels. Aspiration was applied by setting a positive flow rate of 0.25 μL s^{-1}, thus generating negative pressure and drawing the precursor gels into the needle, while expelling the excess casting fluid. Once the gel was almost fully drawn into the needle, the positive flow rate was stopped. Next, a negative flow rate of 2 μL s^{-1} generating positive pressure was applied to controllably eject the compacted DF gels.

Plastic compression-generated dense fibrin gels

Plastic compression was applied to generate dense fibrin (PC-DF) gels, as previously described [34]. Briefly, precursor gels were subjected to a 1 kPa compressive stress for 5 min to expel the casting fluid and generate PC-DF gels (Fig. 7).

Determination of gel compaction factor and fibrin fibrillar density

The compaction factor in generating GAE-DF gels was defined as the surface area reduction (SAR%), which is the ratio between the cross-sectional surface areas of the precursor gel (SAi) and needle (SAf) used in automated GAE and calculated according to Eq. (1) [43] as follows:

$$\mathrm{SAR} = \frac{(\mathrm{SAi} - \mathrm{SAf})}{\mathrm{SAi}} 100 \tag{1}$$

Using Eq. (1), needle gauge numbers of 8G and 12G resulted in SAR values of 88 and 95%, respectively.

Fibrin fibrillar density of the gels ($n = 3$) was determined through their dry-to-wet weight ratio ($n = 5$) [34]. The as-made gels were freeze-dried overnight at − 104 °C and 14 mTorr (Bench-Top K VirTis, USA). Weight percent of fibrin in the gels was calculated according to Eq. (2) [34] as follows:

$$\text{Fibrin fibrillar density} = \frac{W[\mathrm{dry}]}{W[\mathrm{wet}]} \times 100. \tag{2}$$

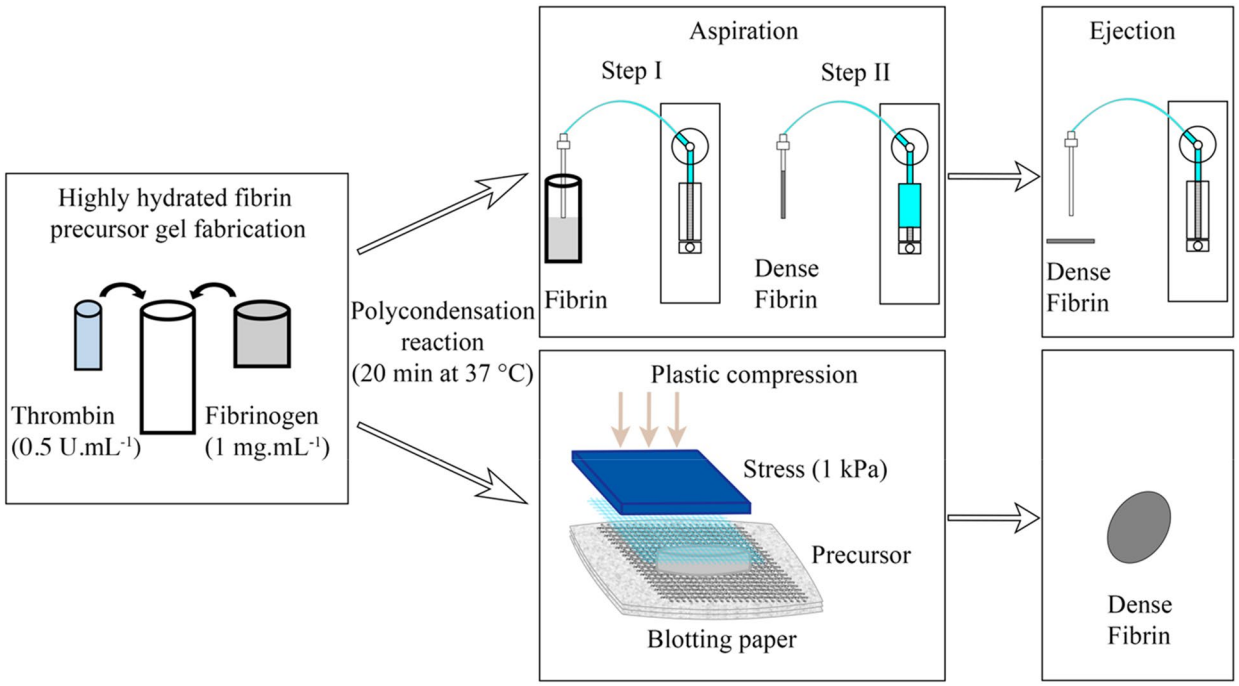

Figure 7: Fabrication of dense fibrin gels. Precursor gel is cast into a 48-well plate mould at 37 °C for 20 min. Following, the precursor gel is processed either through automated GAE or plastic compression. Processing through automated GAE of precursor gel (top row) is performed with a system consisting of a syringe pump connected to different gauge number needles through Luer locks. The aspiration of the gel into the needle rapidly expels the casting fluid, which is then controllably ejected (Video S1 provides more information about the process). Processing through plastic compression (bottom row) is performed by placing the precursor gel between two meshes, then a load is applied atop to rapidly expel the casting fluid which is absorbed by the blotting paper placed underneath.

Culturing of seeded MSCs in GAE-DF and PC-DF gels

Passage 9 mouse C57BL/6 bone marrow-derived MSCs (Life technologies; Gibco, Canada) were incubated at 5% CO_2 and grown to 80% confluency at 37 °C. The expansion and growth medium consisted of Dulbecco's modified essential medium F12 (DMEM/F12, Life technologies; Gibco, Canada) supplemented with 10% foetal bovine serum (FBS, HyClone, Canada) and 5 μg mL^{-1} gentamicin antibiotic (Life technologies, Canada). Precursor fibrin gels were processed by transferring 1.5 mL of fibrin solution seeded with MSCs at a density of 2×10^5 cells mL^{-1} into a 48-well plate and cast in an incubator with 5% CO_2 atmosphere at 37 °C for 30 min. MSC-seeded GAE-DF with SAR of 88% and 95% were compared to those seeded in PC-DF. Culturing was carried out in either growth medium (basal) or in osteogenic differentiation medium that consisted of DMEM/F12 supplemented with 50 μg mL^{-1} of ascorbic acid, 10 mM β-glycerophosphate and 1 μM dexamethasone (all suitable for use in tissue culture system, Sigma-Aldrich, Canada) for up to 28 days. Both basal and osteogenic media were supplemented with 0.1 U mL^{-1} aprotinin (Sigma-Aldrich, Canada) and changed at 2-day intervals.

Seeded MSC viability

Confocal laser scanning microscopy (CLSM; Carl Zeiss LSM510, Germany) was used to image seeded MSC viability and morphology at days 1, 7 and 21 in culture. Seeded cells were stained with 2 μM calcein AM solution (*i.e.* in PBS or culture media) (Life Technologies, Canada) and incubated at 37 °C for 15 min prior to viewing. Excitation and emission wavelengths of 490 and 530 nm, respectively, were used to visualize the stained cells by plane scanning. The resulting emissions from the stain were detected for image assembly.

Determination of cell-induced gel contraction

Cell-induced contraction of gels was assessed on free-floating gels ($n = 3$) to allow for unconstrained contraction. Cell-induced contraction was assessed up to 21 days in culture under basal and osteogenic media. Samples were imaged with a camera (Canon rebel T3) and the results quantified using ImageJ (NIH, USA) with the Fiji open-source plug-in [83]. The initial surface area, as measured from the image of each individual sample was considered equal to its 100%. Then, further images were captured at 3-day intervals, and their corresponding surface areas were measured and compared with the initial surface area value to determine the extent of gel contraction. Acellular gels were used as control.

Seeded MSC metabolic activity

The alamarBlue® assay (Life Technologies, Canada) was used to investigate the metabolic activity of seeded MSCs as an indicator of cell viability and proliferation [84]. Specimens ($n = 3$) were incubated for 4 h under darkness in 5% CO_2 and 37 °C in growth medium with 10% alamarBlue® reagent. Post incubation, 100 μL aliquots of media were collected in triplicate. Fluorescence intensity was measured with a Mithras LB940 Multimode Microplate Reader (Berthold Technologies, Germany) equipped with a 555/580 nm filter pair, as an expression of cellular reduction according to the resazurin indicator. Analysis was carried out at days 1, 7, 14 and 21 and plotted against the florescence intensity, which was proportional to the magnitude of metabolic activity. Fluorescence intensity from acellular gels were subtracted from values obtained for cell-seeded gels.

Seeded MSC gene expression

Quantitative polymerase chain reaction (q-PCR) was conducted to amplify alkaline phosphatase (*Alp*), runt-related transcription factor 2 (*Runx2*), osteocalcin (*Ocn*) and collagen type I alpha 1 chain (*Col1a1*) transcripts as indicators of MSC osteogenic differentiation. Primer sequences and amplicon sizes are provided in Table 1. Specimens ($n = 3$) cultured in both basal and osteogenic media were subjected to the PureLink® RNA kit (Life Technologies, Canada). This generated RNA transcripts that were reverse transcribed to cDNA by qScript™ cDNA synthesis kit (Quanta Bioscience Inc.) as per the manufacturer's instruction. PerfeCTa® SYBR® Green FastMix®^{ROX} (Quanta Bioscience Inc.) q-PCR master mix and primer pairs (300 nM each) were prepared for entry into the 7900HT q-PCR thermocycler (Applied Biosystems, USA). Cycling conditions were as follows: an initial denaturation of 95 °C for 10 min, followed by 40 repeats of 95 °C of denaturation for 15 s and an annealing/extension phase of 45 s. Using the $2^{-\Delta\Delta Ct}$ method, data were normalized to the expression of *Gapdh* and calibrated to the day 1 time point.

TABLE 1: Primer sequences and amplicon size used for q-PCR.

Gene	Primers	Amplicon size (base pairs)
Gapdh	(+) 5′—AAG GGC TCA TGA CCA CAG TC—3′	111
	(–) 5′—CAG GGA TGA TGT TCT GGG CA—3′	
Alp	(+) 5′—GGG AGA TGG TAT GGG CGT CT—3′	117
	(–) 5′—AGG GCC ACA AAG GGG AAT TT—3′	
Runx2	(+) 5′—ATC CCC ATC CAT CCA TCC CTC CA—3′	168
	(–) 5′—CTG TCT GTG CCT TCT GGG TT—3′	
Ocn	(+) 5′—GAC AAA GCC TTC ATG TCC AAG C—3′	129
	(–) 5′—AGC AGG GTC AAG CTC ACA TAG—3′	
Col1a1	(+) 5′—GAC GCC ATC AAG GTC TAC TG—3′	154
	(–) 5′—ACG GGA ATC CAT CGG TCA—3′	

Protein analysis (Western blot)

The protein extracts (200 µL) from samples ($n = 3$) were ethanol-precipitated and resuspended in NuPage LDS Loading Buffer (Life Technology), as previously described [85]. The total protein in the extracts was determined by a Pierce Coomassie (Bradford) Protein Assay Kit (Thermo Fisher Scientific Inc., Canada). The proteins were separated on 10% LDS polyacrylamide gels and electrotransferred to an Amersham proton 0.2 nitrocellulose membrane (Hybond-P, GE Healthcare, Canada). The membranes were blocked with 3% skim milk and probed with antibodies against mouse osteopontin (OPN) (R&D Systems, USA) at 1:1000 dilution. An appropriate secondary antibody (R&D) Systems, USA) at a 1:1000 dilution was used. All membranes were developed using a Western Lightning Plus-ECL (PerkinElmer Life Sciences) and LAS 4000 Image Quant system (General Electric). Densitometric calculations were carried out using ImageLab software (Bio-Rad). The samples were normalized to Actin and to the background of the blot.

Scanning electron microscopy (SEM) and image analysis

SEM was used to investigate the microstructure of gels as well as mineral deposition in MSC-seeded gels. Acellular gels were fixed in 4% paraformaldehyde for 30 min (cell-seeded gels overnight) followed by dehydration through a graded series of ethanol solutions, and by chemical drying using 1,1,1,3,3,3-hexamethyldisilazane (Sigma-Aldrich, Canada). SEM analysis was performed on Pt sputter-coated samples (Leica Microsystems EM ACE600 High Resolution Coater, Austria) with a Field Emission-SEM (FEI Inspect F-50 FE-SEM, The Netherlands) at 5 kV and 10 mA with a working distance of 10 mm.

SEM generated images were analysed for fibril directionality through ImageJ (NIH, USA) with the Fiji open-source plug-in [83]. The analysis was carried out using the directionality analysis tool within the applet and selecting the "local gradient orientation" algorithm. The analysis provided a histogram with a dominant Gaussian distribution of fibre directionality analysed from 4 independent SEM images.

Mechanical analysis

Tensile testing was carried out on gel specimens ($n = 5$) mounted into the grippers of a Univert mechanical testing instrument (CellScale Biomaterials, Canada) [34]. Wet specimens were first clamped to the upper plastic gripper of the instrument which was then lowered until the other extremity of the gel landed inside the bottom gripper that was then closed, thus securely fixing the specimen without applying any strain. Tests were performed with a 10 N load cell and a controlled displacement rate of 0.1 mm s^{-1}. The initial load versus displacement data were processed to generate corresponding stress–strain curves by using the needle internal diameter (3.43 and 2.16 mm corresponding to 8G and 12G, respectively) or PC-DF roll diameter (2 mm) as the nominal diameter of each gel, respectively. The ultimate tensile strength (UTS) and apparent modulus were calculated as the maximum stress point and the slope of the linear region, respectively, of the stress–strain curves.

Attenuated total reflectance-fourier transform infrared spectroscopy (ATR-FTIR)

ATR-FTIR spectroscopy was used to characterize the structural properties of as-made gels as well as the mineralization potential of acellular and MSC-seeded gels at day 28 in culture. Samples were fixed overnight in 4% paraformaldehyde, rinsed twice in PBS and finally washed three times in deionized water (DIW) before freeze-drying overnight at − 104 °C and 14 mTorr (BenchTop K freeze-dryer). Spectra were collected (Spectrum 400, PerkinElmer, USA) using a resolution of 2 cm^{-1}, an infrared range of 4000–650 cm^{-1} and 64 scans. Spectra were then corrected with a linear baseline and normalized (absorbance of Amide I at 1643 $cm^{-1} = 1.5$) using Spectrum software (PerkinElmer, USA). Changes in absorption bands related to phosphorous species have been considered as an indication of mineral deposition [41].

X-ray diffraction (XRD)

XRD was used to characterize the as-made as well as the mineralization potential of acellular and MSC-seeded gels at day 28 in culture. Samples were fixed overnight in 4% paraformaldehyde, rinsed twice in PBS and finally washed three times in DIW before freeze-drying overnight at − 104 °C and 14 mTorr (BenchTop K freeze-dryer). The XRD patterns were generated using a Bruker D8 Discover (Germany), a range from 6° to 60° 2θ at 40 kV and 40 mA. Three frames of 23° were recorded for 9 min and merged during data post processing. The International Centre for Diffraction Data (ICDD) database was used to identify the phase composition.

Statistical analysis

Fibre dispersion angles in gels were statistically compared using ordinary one-way analysis of variance. Statistical analysis on all other analyses was performed using a multiple t test with a significance level $p < 0.05$.

Acknowledgments

Funding from NSERC, FRQNT, CFI, McGill Faculty of Engineering Hatch Faculty Fellowship and MEDA are gratefully acknowledged.

Declarations

Conflict of interest GG and SNN are named inventors of PCT /2019/051867: Systems and methods for making biomaterials with target properties.

Supplementary Information

The online version contains supplementary material available at https://doi.org/10.1557/s43578-021-00433-w.

References

1. J. Henkel, M.A. Woodruff, D.R. Epari, R. Steck, V. Glatt, I.C. Dickinson, P.F.M. Choong, M.A. Schuetz, D.W. Hutmacher, Bone regeneration based on tissue engineering conceptions—a 21st century perspective. Bone Res. **1**(3), 216–248 (2013)
2. A.R. Amini, C.T. Laurencin, S.P. Nukavarapu, Bone tissue engineering: recent advances and challenges. Crit. Rev. Biomed. Eng. **40**(5), 363–408 (2012)
3. V. Karageorgiou, D. Kaplan, Porosity of 3D biomaterial scaffolds and osteogenesis. Biomaterials **26**(27), 5474–5491 (2005)
4. T.N. Vo, F.K. Kasper, A.G. Mikos, Strategies for controlled delivery of growth factors and cells for bone regeneration. Adv. Drug Deliv. Rev. **64**(12), 1292–1309 (2012)
5. D.B. Kolesky, R.L. Truby, A.S. Gladman, T.A. Busbee, K.A. Homan, J.A. Lewis, 3D bioprinting of vascularized, heterogeneous cell-laden tissue constructs. Adv. Mater. **26**(19), 3124–3130 (2014)
6. N.E. Fedorovich, J. Alblas, W.E. Hennink, F.C. Öner, W.J.A. Dhert, Organ printing: the future of bone regeneration? Trends Biotechnol. **29**(12), 601–606 (2011)
7. L.L. Hench, J.M. Polak, Third-generation biomedical materials. Science **295**(5557), 1014 (2002)
8. L.F. Brown, N. Lanir, J. McDonagh, K. Tognazzi, A.M. Dvorak, H.F. Dvorak, Fibroblast migration in fibrin gel matrices. Am. J. Pathol. **142**(1), 273–283 (1993)
9. N. Laurens, P. Koolwijk, M.P. de Maat, Fibrin structure and wound healing. J. Thromb. Haemost. **4**(5), 932–939 (2006)
10. M.D. Bale, P.A. Janmey, J.D. Ferry, Kinetics of formation of fibrin oligomers. II. Size distributions of ligated oligomers. Biopolymers **21**(11), 2265–2277 (1982)
11. S. Jockenhoevel, G. Zund, S.P. Hoerstrup, K. Chalabi, J.S. Sachweh, L. Demircan, B.J. Messmer, M. Turina, Fibrin gel—advantages of a new scaffold in cardiovascular tissue engineering. Eur. J. Cardiothorac. Surg. **19**(4), 424–430 (2001)
12. D.H. Sierra, Fibrin sealant adhesive systems: a review of their chemistry, material properties and clinical applications. J. Biomater. Appl. **7**(4), 309–352 (1993)
13. S. Soumya, P.R. Sreerekha, D. Menon, S.V. Nair, K.P. Chennazhi, Generation of a biomimetic 3D microporous nanofibrous scaffold on titanium surfaces for better osteointegration of orthopedic implants. J. Mater. Chem. **22**(5), 1904–1915 (2012)
14. S.-W. Kang, J.-S. Kim, K.-S. Park, B.-H. Cha, J.-H. Shim, J.Y. Kim, D.-W. Cho, J.-W. Rhie, S.-H. Lee, Surface modification with fibrin/hyaluronic acid hydrogel on solid-free form-based scaffolds followed by BMP-2 loading to enhance bone regeneration. Bone **48**(2), 298–306 (2011)
15. J.T. Schantz, S.H. Teoh, T.C. Lim, M. Endres, C.X.F. Lam, D.W. Hutmacher, Repair of calvarial defects with customized tissue-engineered bone grafts. I. Evaluation of osteogenesis in a three-dimensional culture system. Tissue Eng. **9**(Suppl 1), S113–S126 (2003)
16. I. Catelas, N. Sese, B.M. Wu, J.C.Y. Dunn, S. Helgerson, B. Tawil, Human mesenchymal stem cell proliferation and osteogenic differentiation in fibrin gels in vitro. Tissue Eng. **12**(8), 2385–2396 (2006)
17. L. Trombi, D. D'Alessandro, S. Pacini, B. Fiorentino, M. Scarpellini, R. Fazzi, S. Galimberti, S. Guazzini, M. Petrini, Good manufacturing practice-grade fibrin gel is useful as a scaffold for human mesenchymal stromal cells and supports in vitro osteogenic differentiation. Transfusion **48**(10), 2246–2251 (2008)
18. M. Cole, S. Cox, E. Inman, C. Chan, M. Mana, S. Helgerson, B. Tawil, Fibrin as a delivery vehicle for active macrophage activator lipoprotein-2 peptide: In vitro studies. Wound Repair Regen. **15**(4), 521–529 (2007)
19. W.D. Spotnitz, Fibrin sealant: the only approved hemostat, sealant, and adhesive—a laboratory and clinical perspective. ISRN Surg. 203943 (2014)
20. E. Seebach, H. Freischmidt, J. Holschbach, J. Fellenberg, W. Richter, Mesenchymal stroma cells trigger early attraction of M1 macrophages and endothelial cells into fibrin hydrogels, stimulating long bone healing without long-term engraftment. Acta Biomater. **10**(11), 4730–4741 (2014)
21. S.J. Kim, J.D. Jang, S.K. Lee, Treatment of long tubular bone defect of rabbit using autologous cultured osteoblasts mixed with fibrin. Cytotechnology **54**(2), 115–120 (2007)
22. B.W. Park, E.J. Kang, J.H. Byun, M.G. Son, H.J. Kim, Y.S. Hah, T.H. Kim, B. Mohana Kumar, S.A. Ock, G.J. Rho, In vitro and in vivo osteogenesis of human mesenchymal stem cells derived from skin, bone marrow and dental follicle tissues. Differentiation **83**(5), 249–259 (2012)

23. A. Mol, M.I. Van Lieshout, C.G. Dam-De Veen, S. Neuenschwander, S.P. Hoerstrup, F.P.T. Baaijens, C.V.C. Bouten, Fibrin as a cell carrier in cardiovascular tissue engineering applications. Biomaterials **26**(16), 3113–3121 (2005)
24. U. Kneser, A. Voogd, J. Ohnolz, O. Buettner, L. Stangenberg, Y.H. Zhang, G.B. Stark, D.J. Schaefer, Fibrin gel-immobilized primary osteoblasts in calcium phosphate bone cement: in vivo evaluation with regard to application as injectable biological bone substitute. Cells Tissues Organs **179**(4), 158–169 (2005)
25. A. Arkudas, J. Tjiawi, O. Bleiziffer, L. Grabinger, E. Polykandriotis, J.P. Beier, M. Stürzl, R.E. Horch, U. Kneser, Fibrin gel-immobilized VEGF and bFGF efficiently stimulate angiogenesis in the AV loop model. Mol. Med. **13**(9–10), 480–487 (2007)
26. C.S. Linsley, B.M. Wu, B. Tawil, Mesenchymal stem cell growth on and mechanical properties of fibrin-based biomimetic bone scaffolds. J. Biomed. Mater. Res. Part A **104**(12), 2945–2953 (2016)
27. M.G. Haugh, S.D. Thorpe, T. Vinardell, C.T. Buckley, D.J. Kelly, The application of plastic compression to modulate fibrin hydrogel mechanical properties. J. Mech. Behav. Biomed. Mater. **16**(1), 66–72 (2012)
28. J.I. Sasaki, T. Matsumoto, S. Imazato, Oriented bone formation using biomimetic fibrin hydrogels with three-dimensional patterned bone matrices. J. Biomed. Mater. Res. Part A **103**(2), 622–627 (2015)
29. T.C. Gamboa-Martínez, V. Luque-Guillén, C. González-García, J.L. Gómez Ribelles, G. Gallego-Ferrer, Crosslinked fibrin gels for tissue engineering: Two approaches to improve their properties. J. Biomed. Mater. Res. Part A **103**(2), 614–621 (2015)
30. C. Wang, W. Huang, Y. Zhou, L. He, Z. He, Z. Chen, X. He, S. Tian, J. Liao, B. Lu, Y. Wei, M. Wang, 3D printing of bone tissue engineering scaffolds. Bioactive Mater. **5**(1), 82–91 (2020)
31. Y. Song, K. Lin, S. He, C. Wang, S. Zhang, D. Li, J. Wang, T. Cao, L. Bi, G. Pei, Nano-biphasic calcium phosphate/polyvinyl alcohol composites with enhanced bioactivity for bone repair via low-temperature three-dimensional printing and loading with platelet-rich fibrin. Int. J. Nanomed. **13**, 505–523 (2018)
32. E.D. Miller, G.W. Fisher, L.E. Weiss, L.M. Walker, P.G. Campbell, Dose-dependent cell growth in response to concentration modulated patterns of FGF-2 printed on fibrin. Biomaterials **27**(10), 2213–2221 (2006)
33. J.A. Phillippi, E. Miller, L. Weiss, J. Huard, A. Waggoner, P. Campbell, Microenvironments engineered by inkjet bioprinting spatially direct adult stem cells toward muscle- and bone-like subpopulations. Stem Cells **26**(1), 127–134 (2008)
34. R.A. Brown, M. Wiseman, C.B. Chuo, U. Cheema, S.N. Nazhat, Ultrarapid engineering of biomimetic materials and tissues: fabrication of nano- and microstructures by plastic compression. Adv. Func. Mater. **15**(11), 1762–1770 (2005)
35. V. Mudera, M. Morgan, U. Cheema, S. Nazhat, R. Brown, Ultrarapid engineered collagen constructs tested in an in vivo nursery site. J. Tissue Eng. Regen. Med. **1**(3), 192–198 (2007)
36. E. Hadjipanayi, V. Mudera, R.A. Brown, Close dependence of fibroblast proliferation on collagen scaffold matrix stiffness. J. Tissue Eng. Regen. Med. **3**(2), 77–84 (2009)
37. E.A. Abou Neel, U. Cheema, J.C. Knowles, R.A. Brown, S.N. Nazhat, Use of multiple unconfined compression for control of collagen gel scaffold density and mechanical properties. Soft Matter **2**(11), 986–992 (2006)
38. H.J. Levis, R.A. Brown, J.T. Daniels, Plastic compressed collagen as a biomimetic substrate for human limbal epithelial cell culture. Biomaterials **31**(30), 7726–7737 (2010)
39. M. Bitar, R.A. Brown, V. Salih, A.G. Kidane, J.C. Knowles, S.N. Nazhat, Effect of cell density on osteoblastic differentiation and matrix degradation of biomimetic dense collagen scaffolds. Biomacromol **9**(1), 129–135 (2008)
40. S.N. Nazhat, E.A. Abou Neel, A. Kidane, I. Ahmed, C. Hope, M. Kershaw, P.D. Lee, E. Stride, N. Saffari, J.C. Knowles, R.A. Brown, Controlled microchannelling in dense collagen scaffolds by soluble phosphate glass fibers. Biomacromol **8**(2), 543–551 (2007)
41. B. Marelli, C.E. Ghezzi, M. James-Bhasin, S.N. Nazhat, Fabrication of injectable, cellular, anisotropic collagen tissue equivalents with modular fibrillar densities. Biomaterials **37**, 183–193 (2015)
42. N.O. Kamranpour, A.K. Miri, M. James-Bhasin, S.N. Nazhat, A gel aspiration-ejection system for the controlled production and delivery of injectable dense collagen scaffolds. Biofabrication **8**(1), 015018 (2016)
43. G. Griffanti, E. Rezabeigi, J. Li, M. Murshed, S.N. Nazhat, Rapid biofabrication of printable dense collagen bioinks of tunable properties. Adv. Func. Mater. **30**(4), 1903874 (2020)
44. C.L. Chiu, V. Hecht, H. Duong, B. Wu, B. Tawil, Permeability of three-dimensional fibrin constructs corresponds to fibrinogen and thrombin concentrations. BioResearch Open Access **1**(1), 34–40 (2012)
45. B.S. Kim, H.M. Sung, H.K. You, J. Lee, Effects of fibrinogen concentration on fibrin glue and bone powder scaffolds in bone regeneration. J. Biosci. Bioeng. **118**(4), 469–475 (2014)
46. Y.-B. Lee, S. Polio, W. Lee, G. Dai, L. Menon, R.S. Carroll, S.-S. Yoo, Bio-printing of collagen and VEGF-releasing fibrin gel scaffolds for neural stem cell culture. Exp. Neurol. **223**(2), 645–652 (2010)
47. R. Sharma, I.P.M. Smits, L. De La Vega, C. Lee, S.M. Willerth, 3D bioprinting pluripotent stem cell derived neural tissues using a novel fibrin bioink containing drug releasing microspheres. Front. Bioeng. Biotechnol. **8**, 57 (2020)
48. E. Abelseth, L. Abelseth, L. De la Vega, S.T. Beyer, S.J. Wadsworth, S.M. Willerth, 3D printing of neural tissues derived

from human induced pluripotent stem cells using a fibrin-based bioink. ACS Biomater. Sci. Eng. **5**(1), 234–243 (2019)
49. E.D. Kozin, N.L. Black, J.T. Cheng, M.J. Cotler, M.J. McKenna, D.J. Lee, J.A. Lewis, J.J. Rosowski, A.K. Remenschneider, Design, fabrication, and in vitro testing of novel three-dimensionally printed tympanic membrane grafts. Hear. Res. **340**, 191–203 (2016)
50. C. Lee, E. Abelseth, L. de la Vega, S.M. Willerth, Bioprinting a novel glioblastoma tumor model using a fibrin-based bioink for drug screening. Mater. Today Chem. **12**, 78–84 (2019)
51. M.J. Buehler, Y.C. Yung, Deformation and failure of protein materials in physiologically extreme conditions and disease. Nat. Mater. **8**(3), 175–188 (2009)
52. C. Storm, J.J. Pastore, F.C. MacKintosh, T.C. Lubensky, P.A. Janmey, Nonlinear elasticity in biological gels. Nature **435**(7039), 191–194 (2005)
53. W. Ho, B. Tawil, J.C.Y. Dunn, B.M. Wu, The behavior of human mesenchymal stem cells in 3D fibrin clots: dependence on fibrinogen concentration and clot structure. Tissue Eng. **12**(6), 1587–1595 (2006)
54. K. Shapira-Schweitzer, D. Seliktar, Matrix stiffness affects spontaneous contraction of cardiomyocytes cultured within a PEGylated fibrinogen biomaterial. Acta Biomater. **3**(1), 33–41 (2007)
55. T. Wakatsuki, M.S. Kolodney, G.I. Zahalak, E.L. Elson, Cell mechanics studied by a reconstituted model tissue. Biophys. J. **79**(5), 2353–2368 (2000)
56. P.W. Jackson, D. Cratchley, The effect of fibre orientation on the tensile strength of fibre-reinforced metals. J. Mech. Phys. Solids **14**(1), 49–64 (1966)
57. A.S. Curry, N.W. Pensa, A.M. Barlow, S.L. Bellis, Taking cues from the extracellular matrix to design bone-mimetic regenerative scaffolds. Matrix Biol. **52–54**, 397–412 (2016)
58. S.M. Willerth, K.J. Arendas, D.I. Gottlieb, S.E. Sakiyama-Elbert, Optimization of fibrin scaffolds for differentiation of murine embryonic stem cells into neural lineage cells. Biomaterials **27**(36), 5990–6003 (2006)
59. J.T. Parsons, A.R. Horwitz, M.A. Schwartz, Cell adhesion: integrating cytoskeletal dynamics and cellular tension. Nat. Rev. Mol. Cell Biol. **11**(9), 633–643 (2010)
60. A.J. Engler, S. Sen, H.L. Sweeney, D.E. Discher, Matrix elasticity directs stem cell lineage specification. Cell **126**(4), 677–689 (2006)
61. B. Trappmann, J.E. Gautrot, J.T. Connelly, D.G.T. Strange, Y. Li, M.L. Oyen, M.A. Cohen Stuart, H. Boehm, B. Li, V. Vogel, J.P. Spatz, F.M. Watt, W.T.S. Huck, Extracellular-matrix tethering regulates stem-cell fate. Nat. Mater. **11**(7), 642–649 (2012)
62. C. Yang, M.W. Tibbitt, L. Basta, K.S. Anseth, Mechanical memory and dosing influence stem cell fate. Nat. Mater. **13**(6), 645–652 (2014)
63. Q. Ye, G. Zünd, P. Benedikt, S. Jockenhoevel, S.P. Hoerstrup, S. Sakyama, J.A. Hubbell, M. Turina, Fibrin gel as a three dimensional matrix in cardiovascular tissue engineering. Eur. J. Cardiothorac. Surg. **17**(5), 587–591 (2000)
64. V. Sacchi, R. Mittermayr, J. Hartinger, M.M. Martino, K.M. Lorentz, S. Wolbank, A. Hofmann, R.A. Largo, J.S. Marschall, E. Groppa, R. Gianni-Barrera, M. Ehrbar, J.A. Hubbell, H. Redl, A. Banfi, Long-lasting fibrin matrices ensure stable and functional angiogenesis by highly tunable, sustained delivery of recombinant VEGF. Proc. Natl. Acad. Sci. USA **111**(19), 6952–6957 (2014)
65. C. Perka, O. Schultz, K. Lindenhayn, R.S. Spitzer, M. Muschik, M. Sittinger, G.R. Burmester, Joint cartilage repair with transplantation of embryonic chondrocytes embedded in collagen-fibrin matrices. Clin. Exp. Rheumatol. **18**(1), 13–22 (2000)
66. D. Dikovsky, H. Bianco-Peled, D. Seliktar, The effect of structural alterations of PEG-fibrinogen hydrogel scaffolds on 3-D cellular morphology and cellular migration. Biomaterials **27**(8), 1496–1506 (2006)
67. M. Köllmer, V. Keskar, T.G. Hauk, J.M. Collins, B. Russell, R.A. Gemeinhart, Stem cell-derived extracellular matrix enables survival and multilineage differentiation within superporous hydrogels. Biomacromol **13**(4), 963–973 (2012)
68. C.L. Cummings, D. Gawlitta, R.M. Nerem, J.P. Stegemann, Properties of engineered vascular constructs made from collagen, fibrin, and collagen-fibrin mixtures. Biomaterials **25**(17), 3699–3706 (2004)
69. V. Serpooshan, M. Julien, O. Nguyen, H. Wang, A. Li, N. Muja, J.E. Henderson, S.N. Nazhat, Reduced hydraulic permeability of three-dimensional collagen scaffolds attenuates gel contraction and promotes the growth and differentiation of mesenchymal stem cells. Acta Biomater. **6**(10), 3978–3987 (2010)
70. V. Serpooshan, N. Muja, B. Marelli, S.N. Nazhat, Fibroblast contractility and growth in plastic compressed collagen gel scaffolds with microstructures correlated with hydraulic permeability. J. Biomed. Mater. Res. Part A **96**(4), 609–620 (2011)
71. F. Chicatun, C.E. Pedraza, C.E. Ghezzi, B. Marelli, M.T. Kaartinen, M.D. McKee, S.N. Nazhat, Osteoid-mimicking dense collagen/chitosan hybrid gels. Biomacromol **12**(8), 2946–2956 (2011)
72. M. Westhrin, M. Xie, M.Ø. Olderøy, P. Sikorski, B.L. Strand, T. Standal, Osteogenic differentiation of human mesenchymal stem cells in mineralized alginate matrices. PLoS ONE **10**(3), e0120374 (2015)
73. L. Malaval, D. Modrowski, A.K. Gupta, J.E. Aubin, Cellular expression of bone-related proteins during in vitro osteogenesis in rat bone marrow stromal cell cultures. J. Cell. Physiol. **158**(3), 555–572 (1994)
74. S. Maxson, K.J.L. Burg, Conditioned media cause increases in select osteogenic and adipogenic differentiation markers in

mesenchymal stem cell cultures. J. Tissue Eng. Regen. Med. **2**(2–3), 147–154 (2008)
75. K.H. Wlodarski, A.H. Reddi, Alkaline phosphatase as a marker of osteoinductive cells. Calcif. Tissue Int. **39**(6), 382–385 (1986)
76. M. Bruderer, R.G. Richards, M. Alini, M.J. Stoddart, Role and regulation of runx2 in osteogenesis. Eur. Cell. Mater. **28**, 269–286 (2014)
77. J.B. Lian, G.S. Stein, J.L. Stein, A.J. Van Wijnen, Osteocalcin gene promoter: Unlocking the secrets for regulation of osteoblast growth and differentiation. J. Cell. Biochem. **72**(Suppl 30/31), 62–72 (1998)
78. L. Masi, A. Franchi, M. Santucci, D. Danielli, L. Arganini, V. Giannone, L. Formigli, S. Benvenuti, A. Tanini, F. Beghe, M. Mian, M.L. Brandi, Adhesion, growth, and matrix production by osteoblasts on collagen substrata. Calcif. Tissue Int. **51**(3), 202–212 (1992)
79. J.Y. Choi, B.H. Lee, K.B. Song, R.W. Park, I.S. Kim, K.Y. Sohn, J.S. Jo, H.M. Ryoo, Expression patterns of bone-related proteins during osteoblastic differentiation in MC3T3-E1 cells. J. Cell. Biochem. **61**(4), 609–618 (1996)
80. D.Z. Bakhyt, L. Wen-Lang, C. Pill-Hoon, S.H.-H. Chien Jaro, T.S. Kuber, C. Moon-Il, Differential induction of bone sialoprotein by dexamethasone and osteogenic protein-1 (OP-1, BMP-7) in rat periodonatal ligament cells in vitro. Int. J. Oral Biol. **23**(2), 91–101 (1998)
81. M.A. Aronow, L.C. Gerstenfeld, T.A. Owen, M.S. Tassinari, G.S. Stein, J.B. Lian, Factors that promote progressive development of the osteoblast phenotype in cultured fetal rat calvaria cells. J. Cell. Physiol. **143**(2), 213–221 (1990)
82. M. Morinobu, M. Ishijima, S.R. Rittling, K. Tsuji, H. Yamamoto, A. Nifuji, D.T. Denhardt, M. Noda, Osteopontin expression in osteoblasts and osteocytes during bone formation under mechanical stress in the calvarial suture In vivo. J. Bone Miner. Res. **18**(9), 1706–1715 (2003)
83. J. Schindelin, I. Arganda-Carreras, E. Frise, V. Kaynig, M. Longair, T. Pietzsch, S. Preibisch, C. Rueden, S. Saalfeld, B. Schmid, J.-Y. Tinevez, D.J. White, V. Hartenstein, K. Eliceiri, P. Tomancak, A. Cardona, Fiji: an open-source platform for biological-image analysis. Nat Methods **9**(7), 676–682 (2012)
84. S. Al-Nasiry, N. Geusens, M. Hanssens, C. Luyten, R. Pijnenborg, The use of Alamar Blue assay for quantitative analysis of viability, migration and invasion of choriocarcinoma cells. Hum. Reprod. **22**(5), 1304–1309 (2007)
85. Y. Oike, K. Kimata, T. Shinomura, K. Nakazawa, S. Suzuki, Structural analysis of chick-embryo cartilage proteoglycan by selective degradation with chondroitin lyases (chondroitinases) and endo-beta-D-galactosidase (keratanase). Biochem. J. **191**(1), 193–207 (1980)